Title: Histone deacetylase 3 regulates microglial function through histone deacetylation

Authors: Laura Meleady[1,2], Morgan Towriss[1,2], Vince Bacarac[1,2], Jennifer Kim[1,3], Megan Rowland[1,2], and Annie Vogel Ciernia[1,2]

1. Djavad Mowafaghian Centre for Brain Health, University of British Columbia, Vancouver, Canada
2. Department of Biochemistry and Molecular Biology, University of British Columbia, Vancouver, Canada
3. Graduate Program in Neuroscience, University of British Columbia, Vancouver, Canada

Correspondence:
Annie Vogel Ciernia
annie.ciernia@ubc.ca

Keywords: microglia, chromatin, gene expression, Hdac3, neuroinflammation

Abstract

Background

As the primary innate immune cells of the brain microglia respond to damage and disease through pro-inflammatory release of cytokines and neuroinflammatory molecules. Histone acetylation is an activating transcriptional mark that regulates gene expression, which is altered in states of disease. Inhibition of histone deacetylase 3 (Hdac3) has been utilized in pre-clinical models of disease to dampen inflammation, but the molecular mechanisms underlying Hdac3's regulation of inflammatory gene expression in microglia is not well understood.

Methods

Functional changes in immortalized microglia were characterized using a Hdac3 specific inhibitor RGFP966 in response to an immune challenge lipopolysaccharide (LPS). Flow cytometry and cleavage under tags & release using nucleases (CUT & RUN) were used to investigate global and promoter-specific histone acetylation changes, resulting in altered gene expression.

Results

Hdac3 inhibition enhanced neuroprotective functions of microglia in response to LPS through reduced nitric oxide release and increased baseline phagocytosis. Inhibition of Hdac3 enhanced histone acetylation globally and at specific gene loci, resulting in the release of gene repression at baseline and enhanced responses to LPS.

Conclusion

The findings suggest Hdac3 serves as a negative regulator of microglial gene expression, and that inhibition of Hdac3 facilitates the microglial response to inflammation and its subsequent resolution. Together, this work provides new mechanistic insights into therapeutic applications of Hdac3 inhibition which mediate reduced neuroinflammatory insults through microglial response.

Background

As the resident immune cells of the brain, microglia are acutely sensitive and respond rapidly to changes in the local brain environment(Gosselin et al., 2014, 2017; Lavin et al., 2014). Due to their ability to respond to a diverse number of stimuli, microglia are involved in virtually all CNS disorders, ranging from degenerative and neurodevelopmental diseases to autoimmune neuroinflammatory conditions (Prinz et al., 2021). Dozens of genetic loci affecting microglial phagocytosis, activation, or immunoregulation have been linked to Parkinson's disease (e.g., TREM2)(Guerreiro et al., 2013), Alzheimer disease (e.g., ABCA7, EPHA1, MS4A6A, CD2AP, CD33)(Hollingworth et al., 2011), frontotemporal dementia (e.g., GRN)(Sims et al., 2017), schizophrenia (e.g., C4)(Sekar et al., 2016), and multiple sclerosis (MS) (e.g., TNFRSF1A, IRF8, CD6)(De Jager et al., 2009; Leppä et al., 2011; Park et al., 2013). Both over and under active microglial phenotypes have been linked to disease pathogenesis across different brain disorders (Prinz et al., 2021). However, it is often unclear if altered microglial activity is helpful or harmful (Prinz et al., 2021), necessitating a deeper understanding of microglial regulation and functional impacts on the brain in both health and disease.

In reaction to an immune insult, microglia rapidly increase expression of inflammatory cytokines and adopt an ameboid morphology, allowing for increased mobility to sites of infection and efficient phagocytosis of infectious agents(Hammond et al., 2018b). This rapid mobilization requires induction of gene expression that is controlled through modifications of chromatin structure via epigenetic mechanisms(Kaikkonen et al., 2013). Epigenetic modifications control gene expression through DNA methylation, histone tail post-translational modifications (acetylation, methylation, phosphorylation, etc.), nucleosome remodeling, and non-coding RNAs. Histone acetylation is also a key marker of active transcription, both at promoters (H3K9ac) and enhancers (H3K27ac). These acetylation marks promote more open chromatin by loosening the interactions between the DNA and histones and also are recognized by bromo domain containing transcriptional activators(Talbert and Henikoff, 2021). Histone acetylation is regulated by two classes of opposing enzymes, histone acetyltransferases (Hats) and Histone deacetylases (Hdacs). Hats add acetyl groups to histone tails, while Hdacs repress

gene expression through removal of acetyl histone modifications. Removal of histone acetylation alters DNA-chromatin electrostatic contacts resulting in compaction of chromatin structure, decreased accessibility for transcription factor binding and inhibition of transcription(Talbert and Henikoff, 2021).

Previous work has explored Hdac3 as a key negative regulator of gene expression in the brain(Mcquown and Wood, 2011). Hdac3 is the only Hdac found in the N-CoR/SMRT complex(Ishii, 2021) and serves as the catalytic component of the complex, leading to histone deacetylation and transcriptional repression. In neurons Hdac3 serves as a negative regulator of activity dependent immediate early gene expression. Genetic deletion or pharmacological inhibition of Hdac3 enhances learning induced gene expression and memory formation in a wide variety of learning paradigms, brain regions and species(Mcquown and Wood, 2011; Vogel-Ciernia and Wood, 2012; Malvaez et al., 2013, 2018; Phan et al., 2017; Kwapis et al., 2018; Campbell et al., 2021). In response to brain damage, translation of Hdac3 is upregulated in both cortical(Zhang et al., 2020) and spinal cord microglia(Kuboyama et al., 2017). In cultured primary microglia, LPS treatment increases Hdac3 protein levels and enzymatic activity within 3 hours and remains elevated for at least 24 hrs(Zhang et al., 2020). *In vivo*, the increase in Hdac3 protein levels appears to confer pro-inflammatory functions(Kuboyama et al., 2017; Zhang et al., 2020). However, activation of microglia during injury can be both beneficial and detrimental as microglia localized to the site of injury promote tissue repair but contribute to secondary damage through release of pro-inflammatory factors. This unique regulation of Hdac3 in microglia supports a critical role for Hdac3 in the regulation of microglial-mediated inflammation and provides a unique opportunity to target Hdac3 clinically to negate the negative impacts of neuroinflammation in brain disease.

Pharmacological inhibition of Hdac3's deacetylase activity reduces neuroinflammation and is protective in models of depression(Bian et al., 2021), stroke(Zhang et al., 2020), and spinal cord injury(Kuboyama et al., 2017; Wahane et al., 2021). General inhibition of class I Hdacs(Hsing et al., 2015) or specifically Hdac3(Bian et al., 2021) can reverse LPS induced sickness behaviour,

weight loss and anhedonia when given just prior to LPS injection. Hdac inhibition also reduced pro-inflammatory cytokine expression in brains and reversed LPS induced microglial morphology changes(Hsing et al., 2015; Bian et al., 2021). Together this suggests a pro-inflammatory role for class I Hdacs in microglial regulation, which is counterintuitive given the canonical role of Hdacs in suppressing inflammatory gene expression. However, given the positive disease modulating impacts of Hdac inhibitors across models of neuroinflammation, understanding how Hdacs regulate immune function is critical for designing better, more specific inhibitors for clinical use. To investigate the potential neuroprotective mechanisms of Hdac3-inhibition, we investigated epigenetic and gene expression shifts in an *in vitro* microglia model of pro-inflammatory response (LPS).

Methods

BV2 Immortalized Microglia Culture

BV2 is a transformed cell line derived from C57BL/6 female (age 1 week) *mus musculus* (mouse) immortalized by recombinant retrovirus J2. Cells were cultured in DMEM/F12, 10% HI-FBS, 1x L-Glutamine (ThermoFisher #25030081), 1x Penicillin-Streptomycin. Before plating cells were trypsinized using 0.25% Trypsin- Ethylenediaminetetraacetic acid (EDTA) (ThermoFisher #25200072) and spun at 300g for 7 minutes, then plated in reduced serum media DMEM/F12 and 2% HI-FBS without antibiotics.

Hdac Inhibitor and LPS Treatments

Hdac Inhibitor drugs RGFP66 (APExBio #A8803) and Suberoylanilide hydroxamic acid (SAHA) (StemCell #73902) were resuspended and stored in DMSO (Cell Signal Technology #12611). BV2 cultures were treated with 15uM RGFP966, 1uM SAHA, or DMSO (vehicle control) for 1 hour. Lipopolysaccharides (LPS) from *Escherichia coli* (SigmaAldrich #L5418) were diluted to 10ng/ml in distilled H_2O (also used as vehicle control). Lipopolysaccharide (LPS) was added at concentrations of 0.01-500ng/mL for 1-, 3-, 6-, or 24-hour incubation.

Immunofluorescent Staining of Cell Culture

Immunofluorescent staining of microglia cultures was performed directly in 8-well chamber slides (MilliporeSigma™ Millicell™ EZ slides #PEZGS0816) pre-coated for 2 hours with poly-D-lysine (Gibco #A3890401). The cells were fixed using 4% paraformaldehyde (PFA) (Alfa Aesar #J61899-AK) for 10 minutes. The cells were washed with phosphate buffered saline (PBS), followed by permeabilization with 0.3% Triton-X100™ (FisherScientific #BP151-500) for 5 minutes. Non-specific antibody binding was blocked for 1 hour using 5% Normal Donkey Serum (NDS) (Jackson ImmunoResearch #017-000-121). A primary antibody was added to blocking buffer overnight at 4°C, washed with PBS and a secondary antibody added for 2 hours. The antibodies used include ionized calcium binding adaptor molecule 1 (IBA1) polyclonal antibody (Invitrogen #PA5-18039) detected using anti-goat IgG, highly cross-absorbed, CF™594 antibody (Millipore Sigma #SAB4600319), HDAC3 Rabbit mAb (Cell Signaling Technology #85057) detected by AlexaFluor® 647 Donkey Anti-Rabbit IgG (Jackson ImmunoResearch #711606152), acetyl-histone H3 (Lys27) Rabbit mAb (Cell Signaling Technology #8173) and acetyl-histone H3 (Lys9) Rabbit mAb (Cell Signaling Technology #9649) detected by AlexaFluor® 647 Donkey Anti-Rabbit IgG (Jackson ImmunoResearch #711606152). Cell nuclei were stained using 4',6-Diamidino-2-Phenylindole (DAPI) (Biolegend #422801) and slides were mounted in VECATSHIELD Antifade mounting medium (FisherScientific #NC9265087).

Reverse Transcription Quantitative Real-Time Polymerase Chain Reaction (RT-qPCR)

Primary rat microglia or BV2 cells were collected in RNA lysis buffer (from Zymo Research Quick-RNA Microprep kit) by gentle pipetting. Lysates were placed on ice and RNA extraction performed using Zymo Research Quick-RNA Microprep kit (Zymo Research #R1051). The RNA was eluted in 30uL nuclease free water and RNA concentration was determined by nanodrop. Complementary DNA (cDNA) was synthesized from 200ng RNA using LunaScript® RT-SuperMix kit (New England Biolabs #E3010) polymerase chain reaction (PCR). RT-qPCR reactions were performed using Luna® Universal qPCR Master Mix (New England Biolabs #M3003). Primers for qPCR reactions were pre-designed by Integrated DNA Technologies for microglia activation and candidate genes (*Il-6, Tnfa, Il-1b, Il-10, Cxcl16, Nr4a2, Arg1, Tlr4*) as well as housekeeping genes

(*Hprt1, Gapdh*). All primer melt curves were evaluated to verify a single product of the predicted size was produced. Primer efficiency was validated by standard curve. Reactions were run in MicroAmp™ Fast Optical 96-Well Reaction Plates (Applied Biosystems #4346907) using Quant-Studio 6 qPCR machine. Reactions were recorded for 40 qPCR cycles (95°C for 15sec, 60°C for 30sec) followed by a primer melt curve. ΔCt values were calculated (Ct gene of interest – Ct housekeeping gene), ΔΔCt values were calculated (ΔCt treatment condition- ΔCt control condition), fold change values were calculated (2^(-ΔΔCt)). In all experiments, the house keeping gene was tested to verify no significant changes across conditions.

Gene Target (mRNA)	**Forward Sequence**	**Reverse Sequence**
Il-6	CGATGATGCACTTGCAGAAA	ACTCCAGAAGACCAGAGGAA
Tnfa	GGGTGATCGGTCCCCAAA	TGAGGGTCTGGGCCATAGAA
Il-1b	TGGCAACTGTTCCTGAACTCA	GGGTCCGTCAACTTCAAAGAAC
Il-10	ACAAAGGACCAGCTGGACAA	TAAGGCTTGGCAACCCAAGTA
Cxcl16	ATCAGGTTCCAGTTGCAGTC	TTCCCATGACCAGTTCCAC
Nr4a2	GTAACTGTAGCTCTGAGAAGCG	CACTGTCCACCTTTAATTTCCTC
Arg1	AGTGTTGATGTCAGTGTGAGC	GAATGGAAGAGTCAGTGTGGT
Tlr4	GACACCAGGAAGCTTGAATCC	GCTGAGTTTCTGATCCATGCA
Nos2	GAGGAGCAGGTGGAAGACTA	GGAAAAGACTGCACCGAAGATA
Hprt1	CAGTACAGCCCCAAAATGGTTA	AGTCTGGCCTGTATCCAACA

Table 1. RT-qPCR Primer Sequences

Cleavage Under Targets & Release Using Nucleases Assay (CUT&RUN)

BV2 microglia (200,000 cells per sample) were collected by trypsinization and pelleting (300g x 6 minutes). CUT & RUN was performed using Cell Signaling Technology CUT & RUN Assay kit (Cell Signaling Technology #86652) according to manufacturer's protocol. Cell pellets were washed, and Concavalin A beads were activated. Bead-bound cells were incubated with primary antibody dilutions overnight at 4°C 1:100 Acetyl-Histone H3 (Lys27) Rabbit mAb (Cell Signaling Technology #8173), 1:50 Acetyl-Histone H3 (Lys9) Rabbit mAb (Cell Signaling Technology #9649), 1:20 negative control Rabbit (DA1E) mAb IgG XP® Isotype Control (Cell Signaling

Technology #66362), and 1:50 positive control Tri-Methyl-Histone H3 (Lys4) Rabbit mAb (Cell Signaling Technology #9751). Bead-cell-antibody samples underwent permeabilization by digitonin buffer, followed by incubation with modified micrococcal nuclease (pAG-MNase) digestion activated by calcium chloride at 4°C for 30 minutes. DNA fragments were released by shaking incubation and isolated using DNA Purification Buffers and Spin Columns (ChIP, CUT&RUN) (Cell Signaling Technology #14209). Yeast spike-in DNA (5ng) was added to each reaction for normalization using Sample Normalization Primer Set (*Act1)* included in assay kit. Positive control antibody H3K4me3 was tested for successful reaction completion using SimpleChIP® Mouse *RPL30* primers included in assay kit. qPCR reactions were performed using Luna® Universal qPCR Master Mix (New England Biolabs #M3003). Reactions were run in MicroAmp™ Fast Optical 96-Well Reaction Plates (Applied Biosystems #4346907) using Quant-Studio 6 qPCR machine. Reactions were recorded for 40 qPCR cycles (95°C for 15sec, 60°C for 30sec) followed by a primer melt curve.

CUT & RUN Primer Design

Primers were designed within the promoter regions (1000bp upstream of transcription start site, TSS) of *Cxcl16, Il-1b, Tlr4, Arg1* and *Arg1.* The University of California Santa Cruz (UCSC) Genome Browser was used to extract genomic sequences of regions of interest. Primers were designed to the sequence using Primer3Web (Version 4.1.0) with primer size 18-23 bp, product size 100-120 base pairs, GC content of 50-70%, and primer melting temperature of 57-62°C. Primers were tested by UCSC Genome Browser In-Silico PCR tool, only primers with one possible product were selected. Primers (DNA oligomers) were ordered from Integrated DNA Technologies and tested by qPCR on genomic mouse DNA, only primers with linear amplification and one product by melt curve analysis were used.

Gene Target	**Forward Sequence**	**Reverse Sequence**
Cxcl16 Promoter	TGCAGGGATGAGAATGGAGG	TGAGTTTTGTGCCCCAGGTA
Tlr4 Promoter	TGCAATGCGTCATCAGTCAG	TGTTTCCTGCAGCTTGTCAT
Il-1b Promoter	TCTCGCCTCCTTGTGCTTAA	AAGTGCGTCTCTCCAGAA

Arg1 Promoter	GCCTCTCTCATCTGCCCTAG	AATCGAAACGGAGCAATGGG
Nos2 Promoter	TAGTGGGGAAATGCTGGTCA	ATATTCCAACACGCCCAGGA

Table 2. CUT & RUN qPCR Primer Sequences

Input Sample Preparation and Analysis of CUT & RUN qPCR Data

Input control samples were prepared for each treatment condition for whole cell chromatin using micrococcal nuclease (Cell Signaling Technology #10011) digestion to mononucleosomes. The isolated DNA was analyzed by bioanalyzer high sensitivity assay, which showed high enrichment for mono-nucleosome sized fragments. qPCR of input samples was run for each qPCR primer set in serial dilutions of 1x, 1:5, 1:25, and 1:125. The Ct values of input serial control dilutions were plotted vs. Log10 (% input) to make a standard curve. The Ct values of antibody-isolated CUT & RUN samples were referenced to standard curve and calculated as percentages (%) of input using the standard curve linear regression. The % of input for each sample was normalized by a factor for the *Act1* yeast-spike in DNA to account for pipetting error. After normalization the % of input for each sample was compared as fold enrichment over the DMSO and H_2O treatment condition. This was repeated for each antibody including the IgG control.

Phagocytosis Assay Quantified by Flow Cytometry

Phagocytic activity of BV2 microglia was detected using engulfment of pHrodo Red *E.coli* BioParticles ™ Conjugate for Phagocytosis (ThermoFisher Scientific #P35361). BV2 microglia (200,000 cells) were plated in 96 well clear round bottom plates. Cells were treated in last hour of incubation with 1:500 dilution of pHrodo red *e.coli* BioParticles ™. Cells were spun 1500rpm for 5 minutes, plate flicked to remove media, washed once in 200uL FACS buffer (500mL Hank's Balanced Salt Solution (HBSS), 0.146g powdered Ethylenediaminetetraacetic acid (EDTA), 10g Bovine Serum Albumin (BSA)). Cells were spun 1500rpm for 5 minutes, plate flicked to remove media and resuspended in 1% PFA for overnight 4°C fixation. The next day cells were washed twice in FACS buffer. Samples were run on the CytoFLEX Flow Cytometer. Flow cytometry data

was analyzed using gating for cell size, granularity, singlet cell population, and phycoerythrin (PE) red-channel signal to detect cells with bead engulfment. Controls run included a no stain control and background PE signal caused by pHrodo Red *E.coli* BioParticles ™ was tested using 2% sodium azide (FisherScientific #BP9221-500) inhibition at 0°C to reduce phagocytosis. FlowJo was used to assess the percent of phagocytic positive cells gated on the no stain in the PE channel and the median fluorescent intensity of the positive population.

Protein Quantified by Flow Cytometry

Global protein concentration of the BV2 cells post treatment was assessed via flow cytometry using intracellular protein staining. BV2 microglia (500,000 cells) were plated in a 12 well untreated cell culture plate in experimental media. Following drug treatment, the cells were removed from the plate using 0.25% trypsin-EDTA and aliquoted into 96 well clear round bottom plates. The cells were fixed and permeabilized using the True-Nuclear Transcription Factor Buffer Set (Biolegend # 424401) according to the manufacturer's instructions. Cells were incubated with primary antibodies for 30 minutes - 1:100 Acetyl-Histone H3 (Lys27) Rabbit mAb (Cell Signaling Technology #8173) or 1:250 Acetyl-Histone H3 (Lys9) Rabbit mAb (Cell Signaling Technology #9649). Antibodies were detected with 1:500 AlexaFluor® 568 Donkey Anti-Rabbit (Invitrogen #A10042) incubated with cells for 30 minutes. Following antibody incubation, cells were spun at 500g for 5 mins and flicked then washed twice with FACS buffer. Cells were run on the CytoFLEX Flow cytometer. FlowJo was used to gate the cells for cell size (FSC A vs SSC A), singlets (FSC-H vs FSC-W), and then for positive signal in the 585 channel to detect antibody fluorescence. Median fluorescence intensity (MFI) for the 585 positive population was used as a measure for protein level. MFIs were normalized to the control condition to determine fold change and compared across conditions.

Griess Reagent Assay

The Griess Reagent kit (ThermoFisher #G7921) was used to quantify nitrite concentrations in media released by BV2 microglia. Griess Reagent was prepared from equal volumes of *N*-(1-naphthyl)ethylenediamine and sulfanilic acid. Microplate assay involved mixing 20uL Griess

Reagent, 150uL nitrite-containing sample (culture supernatant), and 130uL deionized water. The samples were incubated for 30minutes at room temperature alongside a calibration curve of nitrite standards (1-50uM). Absorbance of the nitrite-containing samples was measured at 548nm. A standard curve was prepared from nitrite-containing samples (plotted as nitrite concentrations vs. absorbance). Nitrite concentrations of samples were determined using linear regression of standard curve line.

Statistical Analysis

In instances of one treatment, ordinary one-way ANOVAs were run comparing the mean of each treatment to the control. Dunnett's post hoc comparisons were run for individual treatment comparisons. Residuals were tested for normality using Shapiro-Wilk test. In instances of two treatments (Hdac inhibitor and LPS treatment) a two-way ANOVA was run to fit a full effect model (Hdac inhibitor, LPS treatment and the interaction). Tukey's or Sidak post hoc comparisons were run to compare individual conditions. Residuals were tested for normality using Shapiro-Wilk test. All measures passed normality testing.

Results

BV2 Microglial Cells Response to LPS Treatment

Previous work has assessed the feasibility of BV2 microglia as a robust and model of microglial responses(Anja Henn, Søren Lund, Maj Hedtjärn, André Schrattenholz, Peter Pörzgen, 2009; Pollock et al., 2020). We initially performed a dose curve experiment to assess the gene expression and histone acetylation responses in BV2s to LPS. The expression of interleukin-6 (*Il-6*), tumor necrosis factor alpha (*Tnfa*), and interleukin 1 beta (*Il-1b*) were examined at an LPS range of 10 – 500ng/mL(Kacimi et al., 2011) for a 3-hour duration (**Figure 1A**). A one-way ANOVA revealed a significant effect of LPS on expression of *Il-6* ($F(3,8)=122.0$, $p<0.0001$), *Tnfa* ($F(3,8)=32.95$, $p<0.0001$), and *Il-1b* ($F(3,8)=58.18$, $p<0.0001$), with significant increases in expression of all genes at all timepoints (Dunnett's post hoc comparisons $p<0.05$).

Responsiveness to 10ng/mL LPS was then tested over a time course of 1, 3, 6, and 24 hours (**Figure 1B**) for gene expression of pro-inflammatory cytokines *Il-6, Tnfa, Il-1b*, anti-inflammatory cytokine *Il-10*, chemokine(C-X-C motif) ligand 16 (*Cxcl16*), nuclear receptor subfamily 4 group A member 2 (*Nr4a2*), arginase 1 (*Arg1*), and nitric oxide synthase 2 (*Nos2*). One-way ANOVAs revealed a significant main effect of LPS duration for *Il-6* ($F(4,9)=2293$, $p<0.0001$), *Tnfa* ($F(4,9)=1410$, $p<0.0001$), *Il-1b* ($F(4,9)=1379$, $p<0.0001$), and *Il-10* ($F(4,9)=58.51$, $p<0.0001$), *Cxcl16* ($F(4,9)=32.45$, $p<0.0001$), *Nr4a2* ($F(4,8)=405.4$, $p<0.0001$), *Arg1* ($F(4,9)=52.09$, $p<0.0001$), and *Nos2* ($F(4,9)=269.2$, $p<0.0001$). Dunnett's post hoc comparisons were run for each LPS duration compared to H_2O control and revealed the expected significant increase in cytokine and chemokine expression by 1hr of treatment that largely maintained to 24hrs. *Nr4a2*, a known Hdac3 target gene in neurons, showed a transient increase at 1hr followed by a significant repression at subsequent time points. *Arg1* and *Nos2*, two enzymes that regulate nitric oxide production, showed significant repression at 1hr of LPS. *Arg1* remained below baseline levels while *Nos2* increased above baseline by 6 and 24 hours of treatment.

To examine impact of LPS treatment on histone acetylation, we measured global protein levels of H3K27ac and H3K9ac by intracellular flow cytometry. One way ANOVA revealed a significant with LPS treatment in both H3K27ac ($F(4,29)=19.61$, $p<0.0001$) and H3K9ac ($F(4,19)=6.892$, $p=0.0013$). Dunnett's post hoc comparisons demonstrated a significant increase in H3K27ac by 1 hour of LPS that was consistently increased at 6 and 24 hours. H3K9ac levels were also significantly increased after 6 and 24 hours of LPS. We also examined global levels of Hdac3 protein and found a significant but minor fluctuation in protein levels at 6 hours of LPS ($F(4,9)=11.6$, $p=0.0013$).

Hdac Inhibition Modulates BV2 Microglial Gene Expression

To test the role for Hdac3 in regulating LPS mediated gene expression, we utilized the Hdac3 selective small molecule inhibitor RGFP966 that inhibits the enzymatic activity of Hdac3 (IC_{50}=80nM) with >200-fold selectivity over other Hdacs(Malvaez et al., 2013). As a comparison, we also used the clinically approved pan-Hdac inhibitor SAHA that inhibits all Class I and II

HDACs (HDAC 1-10)(Marks, 2007). Hdac inhibitors were applied to BV2 cultures for 1 hour prior to treatment with either LPS (10ng/ml) or vehicle (water) for 1 or 3 hours (**Figure 2A**). We then examined the mRNA expression of *Il-1b*, *Tnfa, Il-10*, *Cxcl16*, *Nr4a2*, *Arg1*, and *Nos2*.

A two-way ANOVA for *Il-1b* at 1 hour of LPS treatment revealed a significant main effect of LPS ($F(1,18)=834.6$, $p<0.001$), of Hdac inhibition ($F(2,18)=135.1$, $p<0.0001$) and an interaction $F(2,18)=15.55$, $p=0.0001$). At 3 hour of LPS treatment, *Il-1b* showed a significant main effect of LPS ($F(1,18)=2638$, $p<0.001$), of Hdac inhibition ($F(2,18)=285.7$, $p<0.0001$) and but no interaction $F(2,18)=1.461$, $p=0.2581$). Tukey's multiple comparisons revealed a significant increase in *Il-1b* with RGFP966 above vehicle both at baseline and in response to LPS at 1 and 3 hours. This enhancement in expression was not observed with SAHA treatment at 1 hour and a slight increase in baseline at 3 hours, suggesting the increased expression is largely driving by inhibition of Hdac3.

We next investigated the expression of *Tnfa* and found at 1 hour LPS a significant main effect of LPS ($F(1,16)=9439$, $p<0.0001$), Hdac inhibition ($F(2,16)=39.72$, $p<0.001$) but no interaction ($F(2,16)=1.339$, $p=0.2899$). At three hours there was a main effect of LPS ($F(1,18)=728.8$, $p<0.0001$) but no effect of Hdac inhibition ($F(2,18)=3.308$, $p=0.0598$) nor interaction ($F(2,18)=0.1194$, $p=0.8881$). Tukey's posthoc comparisons at 1 hour LPS showed a small but significant decrease in *Tnfa* expression at baseline and with LPS for both RGFP966 and SAHA. All comparisons were no longer significant by 3 hours, indicating that Hdacs are not negative regulators of *Tnfa* expression.

We also examined expression of the anti-inflammatory cytokine *Il-10* and similar to *Il-1b*, we observed largely RGFP966 specific enhancements in gene expression. At 1 hour of LPS treatment there was a significant main effect of LPS ($F(1,18)=56.88$, $p<0.0001$), Hdac inhibition ($F(2,18)=21.69$, $p<0.0001$) and a significant interaction ($F(2,18)=13.64$, $p=0.0002$). At 3 hours of LPS treatment there was a significant main effect of LPS ($F(1,16)=34.72$, $p<0.0001$), Hdac inhibition ($F(2,16)=19.24$, $p<0.0001$) and but no interaction ($F(2,16)=1.228$, $p=0.3191$). Tukey's

posthocs revealed a significant increase in *Il-10* levels at baseline with both RGFP966 and SAHA, but no modulation of LPS induction. In contrast, at 3 hours of LPS there was a significant increase in baseline *Il-10* expression and enhanced response to LPS only with RGFP966. These findings indicate that both pro and anti-inflammatory cytokines are modulated similarly by Hdac3 inhibition.

To further explore the impact on additional gene targets, we examined the chemokine *Cxcl16*. Similar to *Il-1b* and *Il-10*, for *Cxcl16* expression a two way ANOVA at 1 hour of LPS treatment revealed a significant main effect of LPS ($F(1,18)=33.53$, $p<0.0001$), Hdac inhibition ($F(2,18)=151.7$, $p<0.0001$) and a significant interaction ($F(2,18)=4.242$, $p=0.0310$). At 3 hours of LPS treatment, there was also a significant effect of LPS ($F(1,18)=286.0$, $p<0.0001$), Hdac inhibition ($F(2,18)=302.0$, $p<0.0001$) and an interaction ($F(2,18)=21.56$, $p<0.0001$). Tukey's posthocs revealed a significant increase in *Cxcl16* expression both at baseline at both time pointes with Hdac3 inhibition but and minimal impact with SAHA. In response to LPS, only the Hdac3 inhibitor enhanced gene expression beyond levels observed in the DMSO controls, suggesting that Hdac3 may be the predominant regulator of *Cxcl16.*

In contrast, *Nr4a2* expression was modulated by both RGFP966 and SAHA. At 1 hour of LPS, there was a significant main effect of LPS ($F(1,18)=16.23$, $p=0.0008$) and Hdac inhibition ($F(2,18)=68.63$, $p<0.0001$) but no interaction ($F(2,18)=1.404$, $p=0.2713$). At 3 hours of LPS, there was a significant main effect of LPS ($F(1,18)=54.16$, $p<0.0001$) and Hdac inhibition ($F(2,18)=18.69$, $p<0.0001$) and an interaction ($F(2,18)=8.534$, $p=0.0025$). Tukey's posthocs revealed a significant increase in baseline gene expression with both RGFP966 and SAHA at 1 hour of LPS but not 3 hours. In response to LPS at 1 hour there was a significant increase above DMSO-LPS for both Hdac inhibitors. At 3 hours of LPS, the DMSO control showed decreased gene expression relative to baseline, but this repression failed to occur in both Hdac inhibitor treated conditions. Together, this indicates that Nr4a2 is potentially regulated by multiple Hdacs in a bi-directional manner with enhanced baseline expression and impaired LPS mediated repression.

To examine another gene with LPS induced repression, we measured *Arg1* gene expression. At 1 hour of LPS there was not a significant main effect of LPS ($F(1,18)=1.134$, $p=0.3010$), a significant main effect of Hdac inhibition ($F(2,18)=5.057$, $p=0.0181$) and no interaction ($F(2,18)=0.1193$, $p=0.8882$). At 3 hours of LPS, there was a significant effect of LPS ($F(1,18)=26.81$, $p<0.0001$) and of Hdac inhibition ($F(2,18)=24.62$, $p<0.0001$) and a significant interaction ($F(2,18)=4.994$, $p=0.0188$). Tukey's posthocs revealed no significant differences at 1 hour of LPS. At 3 hours, there was no difference at baseline for either Hdac inhibitor compared to vehicle control, but a trend for a decrease with SAHA. In response to 3 hours of LPS, there was a significant repression in the DMSO control and SAHA treated samples, but not in the RGFP966 sample treated with LPS, similar to the failure in gene repression observed for *Nr4a2.*

As Arg1 acts in opposition to iNos (*Nos2*) in the generation of nitric oxide, we also examined impacts on *Nos2* expression. At 1 hour of LPS treatment there was a significant main effect of LPS ($F(1,18)=8.917$, $p=0.0079$) and Hdac inhibition ($F(2,18)=25.00$, $p<0.0001$), but no significant interaction ($F(2,18)=1.364$, $p=0.2809$). Similarly, at three hours of LPS, there was a significant main effect of LPS ($F(1,18)=801.1$, $p<0.0001$) and of Hdac inhibition ($F(2,18)=16.18$, $p<0.0001$), but no interaction ($F(2,18)=0.4633$, $p=0.6365$). Tukey's posthoc comparisons revealed a significant increase in *Nos2* expression at baseline and in response to LPS at 1 hour, an effect not observed with SAHA. At three hours, there was no difference between either Hdac inhibitor treated condition and the respective DMSO controls, indicating the impacts on *Nos2* expression are short lived.

Hdac Inhibition Enhances Histone Acetylation

The Hdac inhibitor impacts on BV2 microglial gene expression both at baseline and in response to LPS, support a model in which increased histone acetylation is permissive for LPS regulated gene expression. Consequent increases in histone acetylation upon Hdac inhibition would then be consistent with the observed pattern of released gene repression at baseline, enhanced LPS induced gene expression and prevention of LPS induced repression of gene expression. To test

this prediction, we first examined global histone acetylation changes in response to Hdac inhibition and LPS treatment by flow cytometry. Global levels of H3K9ac showed a significant main effect of Hdac inhibitor ($F(2,45)=104.18$, $p<0.0001$), LPS treatment ($F(1,45)=11.50$, $p=0.0015$), but no interaction ($F(2,45)=1.304$, $p=0.2814$). H3K27ac also showed a robust increase upon Hdac inhibition with a significant main effect of Hdac inhibitor ($F(2,44)=77.77$, $p<0.0001$), LPS treatment ($F(1,44)=6.841$, $p=0.0122$), and no significant interaction ($F(2,44)=2.999$, $p=0.0601$). Tukey's corrected posthoc comparisons revealed that both Hdac inhibitors significantly increased H3K9ac and H3K27ac at baseline and upon LPS treatment (**Figure 3**).

To examine the link between gene expression and histone acetylation we examined H3K27ac and H3K9ac by CUT&RUN qPCR at the promoters of select genes with expression regulated by Hdac3 inhibition (**Figure 4A**). The positive control H3K4me3 antibody produced significant enrichment over non-immune IgG ($t(6)=2.511$, $p=0.0458$) indicating the CUT&RUN procedure was working as expected. We examined H3K27ac and H3K9ac over the Cxcl16 promoter (**Figure 4B**). There was a significant main effect of Hdac inhibition ($F(1,8)=18.76$, $p=0.0025$) but not for LPS treatment ($F(1,8)=0.3512$, $p=0.5698$) nor for the interaction ($F(1,8)=0.0003$, $p=0.9576$). Sidak corrected posthoc comparisons between RGFP966 and DMSO treated samples revealed a significant increase in H3K27ac promoter signal with Hdac3 inhibition at both baseline and in response to LPS. For H3K9ac over the Cxcl16 promoter, there was a significant main effect of Hdac inhibition ($F(1,8)=33.86$, $p=0.0004$) and for LPS treatment ($F(1,8)=6.101$, $p=0.0387$), but not for the interaction ($F(1,8)=0.2133$, $p=0.6565$). Sidak corrected posthoc comparisons between RGFP966 and DMSO treated samples revealed a significant increase in H3K9ac promoter signal with Hdac3 inhibition at both baseline and in response to LPS.

For the Il1-b promoter H3K27ac levels, we found a significant main effect of Hdac inhibition ($F(1,8)=11.99$, $p=0.0085$), but no effect of LPS ($F(1,8)=0.2425$, p-0.6356) nor interaction ($F(1,8)=0.048$, $p=0.8314$). H3K9ac levels showed a similar pattern over the Il1b-promoter with a significant main effect of Hdac inhibition ($F(1,8)=8.440$, $p=0.0187$), no effect of LPS

($F(1,8)=0.773$, $p=0.4047$) nor interaction ($F(1,8)=0.003$, $p=0.9571$). Sidak corrected posthocs for both H3K27ac and H3K9ac, revealed trends towards enhanced H3K27ac signal over the promoter at baseline and with LPS (**Figure 4C**).

At the Arg1 promoter, H3K27ac levels showed a significant main effect of Hdac inhibition ($F(1,8)=21.25$, $p=0.0017$), no effect of LPS ($F(1,8)=0.7804$, $p=0.4028$) and no interaction ($F(1,8)=0.4074$, $p=0.5411$). For H3K9ac, there was a significant main effect of Hdac inhibition ($F(1,8)=6.237$, $p=0.0371$), no effect of LPS ($F(1,8)=0.2290$,$p=0.6451$) and no interaction ($F(1,8)=0.1136$, $p=0.7447$). Sidak corrected posthocs revealed a significant increase in H3K27ac signal with RGFP966 over DMSO at both baseline and in response to LPS. Similar trends in increase were also observed for H3K9ac, but did not reach significance (**Figure 4D**). At the Nos2 promoter, H3K27ac levels showed a significant main effect of Hdac inhibition ($F(1,8)=15.10$, $p=0.0046$), no effect of LPS ($F(1,8)=3.112$, $p=0.1157$) and no interaction ($F(1,8)=1.392$, $p=0.2719$). For H3K9ac, there was a significant main effect of Hdac inhibition ($F(1,8)=10.75$, $p=0.0112$), no effect of LPS ($F(1,8)=0.1060$,$p=0.7531$) and no interaction ($F(1,8)=0.0043$, $p=0.9493$). Sidak corrected posthocs revealed a significant increase in H3K27ac with RGFP966 upon LPS treatment and a trend at baseline. There were trends for RGFP966 induced increase in H3K9ac at baseline and with LPS, but they did not reach statistical significance (**Figure 4E**).

Hdac Inhibition Enhances Microglial Phagocytosis and Impairs NO Release

To examine how Hdac inhibition may impact microglia function, we examined phagocytosis of pH-rodo E. coli labelled beads. These beads specifically fluoresce when in the low pH environment of the phagolysosome and can then be quantified by flow cytometry. We quantified the impact of Hdac inhibition and LPS treatment on both the percentage of microglia that phagocytose beads and median fluorescence intensity (MFI) of the engulfed beads, a proxy for the number of beads phagocytosed (**Figure 5A**). At three hours of LPS treatment there was no significant impact of LPS ($F(1,36)=0.0796$, $p=0.7795$) or Hdac inhibition ($F(2,36)=3.119$, $p=0.563$) or an interaction $F(2,36)=0.1551$, $p=0.8569$) for the percentage of bead positive microglia. For the MFI there was no significant effect of LPS ($F(1,36)=3.521$, $p=0.0687$) but there

was a significant effect of Hdac inhibition ($F(2,36)=7.990$, $p=0.0013$), an no interaction $F(2,36)=0.5893$, $p=0.5600$) (**Figure 5B**). At 24 hours of LPS treatment, there were more significant impacts on microglial phagocytosis. The percentage of positive microglia showed a significant effect of LPS $F(2,36)=21.64$, $p<0.0001$) and LPS ($F(1,36)=14.28$, $p=0.0006$) and a significant interaction ($F(2,36)=19.21$, $p<0.0001$). For the MFI at 24 hours there was not an effect of LPS ($F(1,36)=0.0004$, $p=0.9851$), but there was a significant effect of Hdac inhibition $F(2,36)=16.31$, $p<0.0001$) and a significant interaction $F(2,36)=13.92$, $p<0.0001$) (**Figure 5C**). Tukey's corrected posthoc comparisons revealed a significant increase in phagocytosis positive microglia with both RGFP966 and SAHA treatment at baseline. There was no difference between Hdac inhibitor treatments with LPS, indicating that Hdac inhibition may drive maximal phagocytosis even without immune stimulation. At 24 hours of LPS treatment, Tukey's corrected posthocs also revealed that Hdac inhibition produced a significant enhancement in the amount of phagocytosis of individual microglia at baseline but not in response to LPS.

To further examine microglia function we measured release of nitric oxide into the media both at 3 hours and 24 hours of LPS treatment. At 3 hours, there were no significant differences between conditions and overall levels of nitric oxide were low. There was no effect of LPS ($F(1,17)=1.033$, $p=0.3237$), Hdac inhibition ($F(2,17)=1.565$, $p=0.2337$) nor interaction ($F(2,17)=1.691$, $p=0.2140$). At 24 hours there was a significant effect of LPS ($F(1,30)=226.9$, $p<0.0001$) of Hdac inhibition ($F(2,30)=41.95$, $p<0.0001$) and a significant interaction ($F(2,30)=20.23$, $p<0.0001$). Tukey's corrected posthocs revealed a significant increase in NO release upon LPS treatment in the DMSO condition. This increase was blunted with SAHA treatment and reduced to baseline levels with RGFP966 (**Figure 5D**).

Discussion

Using BV2 microglial cells and LPS treatments, we developed a robust model to examine how Hdac3 regulates microglial gene expression. The Hdac3 selective inhibitor RGFP966 robustly increased gene expression of numerous cytokines (*Il1-b*, *Il-10*), chemokines (*Cxcl16*) and LPS inducible regulators (*Nr4a2*, *Arg1*, *Nos2*) both at baseline and in response to LPS. These

responses were not universal as *Tnfa* was not modulated by RGFP966 nor SAHA. Increases in gene expression were paralleled by global and promoter specific increases in H3K27ac and H3K9ac with RGFP966 treatment, supporting the role of Hdac3 as a negative regulator of histone acetylation in microglia. Hdac3 inhibition also had impacts on phagocytosis and NO release after 24 hours, with increases in phagocytosis and strong suppression of NO release. Together, our data indicate that Hdac3 acts as a repressor of histone acetylation and gene expression in microglia, but that the gene targets include both enhancers and suppressors of the inflammation response (Figure 6).

Pharmacological inhibition of Hdac3's deacetylase activity reduces neuroinflammation and is protective in models of depression(Bian et al., 2021), stroke(Zhang et al., 2020), and spinal cord injury(Kuboyama et al., 2017; Wahane et al., 2021). Conditional deletion of Hdac3 in microglia shifted microglial responses to a traumatic brain injury towards a more inflammation resolving phenotype and improved functional recovery(Zhao et al., 2022). Together this suggests a pro-inflammatory role for Hdac3 in regulating microglial function and that suppression of Hdac3 is beneficial for combating neuroinflammation. Our findings indicate that the beneficial effects of inhibiting Hdac3 may be due to several functions of Hdac3 in microglia. We found that inhibition of Hdac3 enhanced phagocytosis while simultaneously blunted NO release. While classically considered a pro-inflammatory response, enhanced phagocytosis following injury or acutely during disease is often beneficial for clearing dead or dying cells in the brain. Augmenting this microglial response may ultimately facilitate brain recovery after damage. RGFP966 suppression of NO release from microglia may further promote resolution of inflammation by damping downstream NO induced pro-inflammatory signals.

Our gene expression findings indicate that RGFP966 may regulate NO release through control of expression of *Arg1* and *Nos2* (iNos). The enzymatic processes of Arg1 and iNos compete for the substrate L-arginine with opposing cellular phenotypes (Cherry et al., 2014). Arg1 hydrolyzes L-arginine to produce urea and L-ornithine, which removes nitrogen from amino acid metabolism via the urea cycle and promotes cell proliferation(Yang and Ming, 2014). The substrate L-

arginine is also used by inducible nitric oxide synthase (iNos) in the production of L-citrulline and NO. We found a decrease in *Arg1* expression with LPS treatment across timepoints. This would effectively decrease competition for L-arginine, allowing iNos to increase production of NO, as we observed in DMSO treated cells upon LPS. RGFP966 effectively prevented the decrease in *Arg1* expression and had only marginal impacts on *Nos2* expression after 3 hours, potentially shifting the microglial activation state away from NO production. This would be consistent with the overall protective effect of RGFP966 in the context of stroke(Zhang et al., 2020) and spinal cord injury(Kuboyama et al., 2017; Wahane et al., 2021).

Hdac3 regulates a diverse repertoire of cellular processes, including differentiation, proliferation, apoptosis, metabolism and inflammation(Karagianni and Wong, 2007). We found that Hdac3 targets both classically anti-inflammatory (*Il-10*) and pro-inflammatory (*Il-1b* but not *Tnfa*) cytokines. The specificity of the regulation does not come from Hdac3, as it does not contain a DNA binding domain but is instead is targeted to specific genes as part of a larger repressor complex that includes nuclear receptor corepressor (N-CoR) and silencing mediator for retinoid and thyroid hormone receptors (SMRT)(Li et al., 2000; Guenther et al., 2001; Karagianni and Wong, 2007). The genomic targeting specificity may stem from interactions with cell type specific transcription factors. In peripheral macrophages, Hdac3 deacetylates a subset of enhancers(Mullican et al., 2011) bound by PU.1, a key macrophage lineage determining transcription factor. Loss of Hdac3 leads to hyperacetylation of thousands of PU.1 enhancers(Chen et al., 2012), demonstrating a role for Hdac3 in controlling immune activity dependent enhancer deacetylation. PU.1 is also a critical transcription factor in microglia(Kierdorf et al., 2013), and future work will be needed to parse direct or indirect interactions between PU.1 and the N-CoR/SMRT/Hdac3 complex in microglia.

In other brain cells such as neurons, Hdac3 has been proposed as “brake” on gene expression through histone deacetylation (McQuown and Wood, 2011). However, in macrophages loss of Hdac3 produces complex impacts on gene expression. Consistent with a proposed role as a negative regulator, loss of Hdac3 in lung macrophages or cultured bone marrow derived

macrophages (BMDM) increases expression of genes that promote wound-healing(Mullican et al., 2011). Hdac3 has also been shown to supress downstream regulators of LPS induced gene expression such as P*tgs1* (Cox-1)(Chen et al., 2012). Similar to our findings with LPS, Hdac3 inhibition significantly increased baseline expression of genes that were normally downregulated by LPS stimulation in BMDM(Ghiboub et al., 2020) and the deacetylase activity of Hdac3 is required for suppressing LPS induced gene expression(Nguyen et al., 2020).

Paradoxically, macrophage Hdac3 also promotes activation of inflammatory gene expression(Chen et al., 2012; Nguyen et al., 2020). Recent work from the Lazar lab demonstrated that in response to LPS, Hdac3 plays a non-canonical activating role through recruitment of activating transcription factor ATF2. The activating role does not require Hdac3's deacetylase activity, and consequently genetic deletion of Hdac3 results in loss of both the canonical transcriptional repression and the non-canonical transcriptional activating roles. The net result of loss of Hdac3 in macrophages was protective from a lethal dose of LPS, but inhibition of Hdac3 enzymatic activity alone was not sufficient to rescue lethality(Nguyen et al., 2020). Our findings in microglia only directly tested the enzymatic role of Hdac3 in regulating gene expression and future work with conditional deletions of Hdac3 will be required to identify if microglial Hdac3 also has a non-canonical activating function.

Hdac3 can also have indirect regulatory roles on microglial gene expression through deacetylation of a number of non-histone proteins. For example, Hdac3 can deacetylate both the HATs p300(Grégoire et al., 2007) and CBP(Chuang et al., 2006), inhibiting their HAT functions. Hdac3 can also deacetylate NF-kB subunit RelA, promoting its nuclear export and termination of NF-kB signaling(Chen et al., 2001). In a mouse model of stroke, RGFP966 reduced brain damaged and facilitated behavioural recovery by inhibition of the AIM2 inflammasome through enhanced acetylation of STAT1. This suggests that Hdac3 normally represses the AIM2 inflammasome through deacetylation of STAT1(Zhang et al., 2020). Similarly, in macrophages Hdac3 interacts with the transcription factor FOXK1 to regulate expression of STAT1(Yang et al., 2022). Future

work will be needed to evaluate these alternative protein targets of Hdac3 in microglial gene regulation and function.

Hdac3 is not the only important Hdac for microglial gene regulation. Hdac1 and 2 are important during early microglial development for cell survival, but not for maintaining homeostasis in adult microglia(Datta et al., 2018). Loss of microglial Hdac1/2 decreased amyloid load and improved cognitive impairment by enhancing microglial amyloid phagocytosis in a mouse model of Alzehimer's(Datta et al., 2018). Hdac1/2 also facilitates the formation of microglial priming such that loss of microglia Hdac1/2 impairs enhancement of *Il-1b*, *Tnfa* and *Il-10* to multiple LPS injections(Wendeln et al., 2018). In our study we used SAHA, a broader class I and II Hdac inhibitor alongside RGFP966 to interrogate Hdac3 specific impacts compared to other class I Hdacs including Hdac1/2. Both RGFP966 and SAHA globally increased histone acetylation to similar degrees, indicating that the doses used in this study were sufficient to inhibit their respective target enzymes. Generally, the broader inhibition of Hdacs by SAHA resulted in less pronounced changes in gene expression both at baseline and with LPS treatment. By 3 hours LPS stimulation, gene expression responses to SAHA were indistinguishable from DMSO treatment. However, functionally SAHA produced similar enhancements in phagocytosis as RGFP966 and blunted NO release, but to lesser magnitude. Together, these findings indicate that some of the SAHA mediated anti-inflammatory effects are mediated by inhibition of Hdac3, but that the more selective RGFP966 more effectively regulates microglial gene expression and function.

One of the limitations of our study is that all experiments were performed in the BV2 microglial immortalized cell line. While *in vitro* studies provide a number of advantages for high throughput and controlled testing of gene expression mechanisms, *in vitro* regulation does not always recapitulate *in vivo* microglial regulation(Gosselin et al., 2014; Bennett et al., 2018).Henn et. al (2009)(Anja Henn, Søren Lund, Maj Hedtjärn, André Schrattenholz, Peter Pörzgen, 2009) assessed the suitability of BV2 microglia as an alternative model to primary microglia culture, and a mimic of *in vivo* microglia. They found that the majority of genes induced in BV2 cells by

LPS treatment were also induced in primary microglia (90%) and freshly isolated hippocampal microglia (50%), although BV2 microglia gene expression changes were less pronounced than primary microglia. Henn et. al also analyzed BV2 responses in functional assays including NO production as well as signaling to astrocytes in co-culture, which demonstrated similar responses to primary microglia. Given similar functional findings using RGFP966 *in vivo* and recent findings showing altered microglial responses in Hdac3 microglial conditional knockout mice(Kuboyama et al., 2017; Zhang et al., 2020; Bian et al., 2021; Wahane et al., 2021; Zhao et al., 2022), we believe our *in vitro* model captures fundamental gene regulation mechanisms and demonstrates how Hdac3 regulation of microglial gene expression leads to *in vivo* improvements in models with brain inflammation.

Conclusion

Together our findings demonstrate an important role for Hdac3 as a negative regulator of the microglial gene expression response to LPS. Our epigenetic profiling indicates Hdac3 suppresses microglial gene expression through deacetylation of histone targets and specifically acts at the promoters of both classically pro- and anti-inflammatory genes. Inhibition of Hdac3 shifts the microglial LPS response towards resolution of inflammation through enhanced phagocytosis and reduced NO release. Our findings provide mechanistic support a model in which Hdac3 inhibition driven shifts in microglial gene expression and function ultimately conveys neuro-protection in brain injury and disease.

Figures

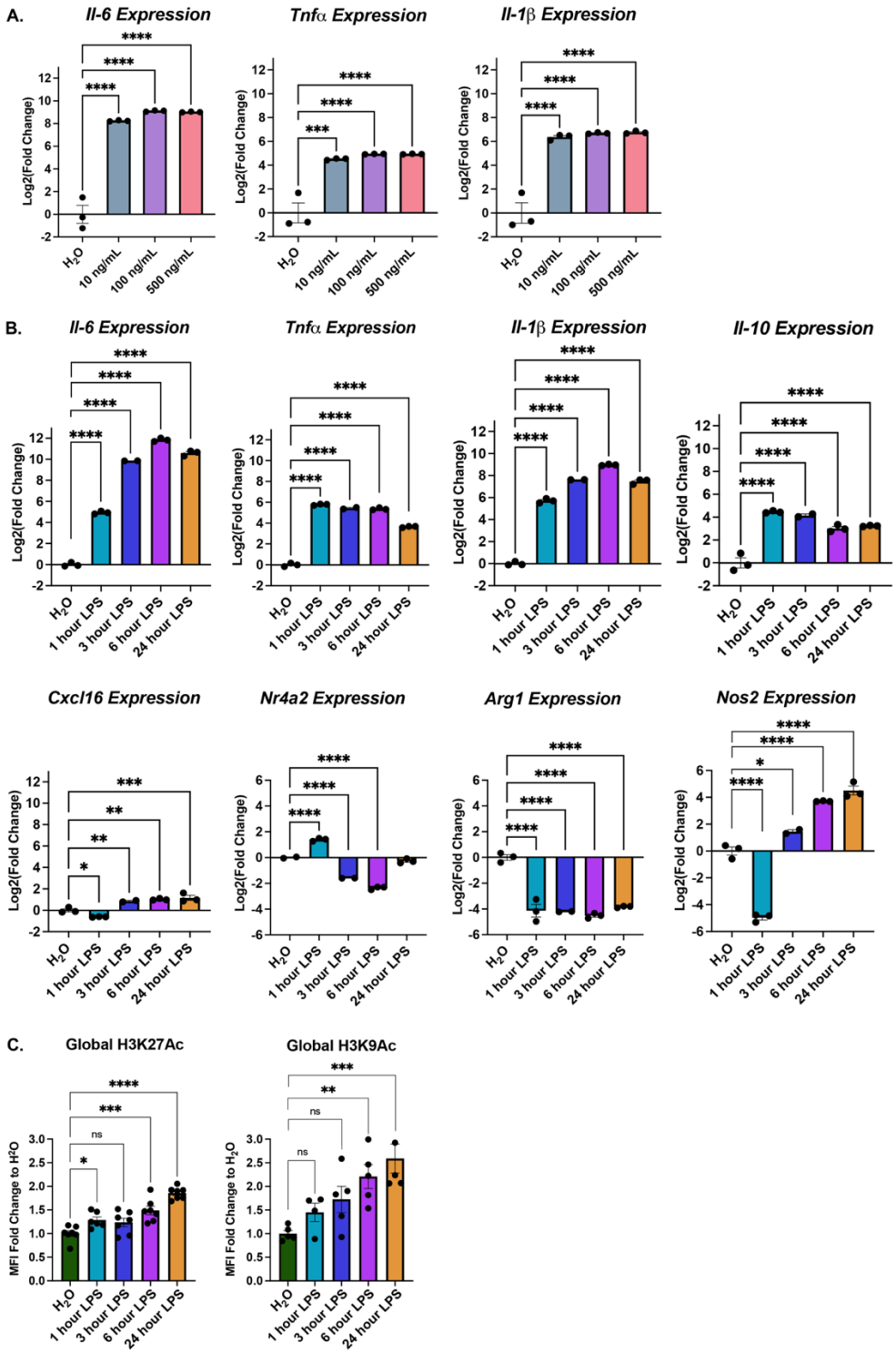

Figure 1. BV2 Immortalized microglia robustly regulate gene expression and histone acetylation to LPS treatment. (A) RT-qPCR assessment of gene expression of *Il-6, Tnfa*, and *Il-1b* in BV2 microglia treated with different LPS doses 10, 100, or 500ng/mL for 3 hours. Shown as bar graph of Log2(Fold Change) ± SEM Dunnett's post hoc significances denoted (*** p<0.0002, **** p<0.0001). (B) RT-qPCR assessment of gene expression of *Il-6, Tnfa*, *Il-1b, Il-10, Cxcl16, Nr4a2, Arg1,* and *Nos2* of BV2 microglia treated with 10ng/mL LPS for 1, 3, 6, or 24 hours.

Shown as bar graph of Log2(Fold Change) ± SEM Dunnett's post hoc significances denoted (*p<0.03, ** p<0.002, *** p<0.0002, **** p<0.0001). (C) Median fluorescent intensity (MFI) for global levels of H3K27ac levels as measured by intracellular flow cytometry. Fold Change ± SEM. Dunnett's post hoc significances denoted (*p<0.05, ** p<0.007, *** p<0.0005, **** p<0.0001). n=2-7 replicates per condition from at least two independent sets of cultures.

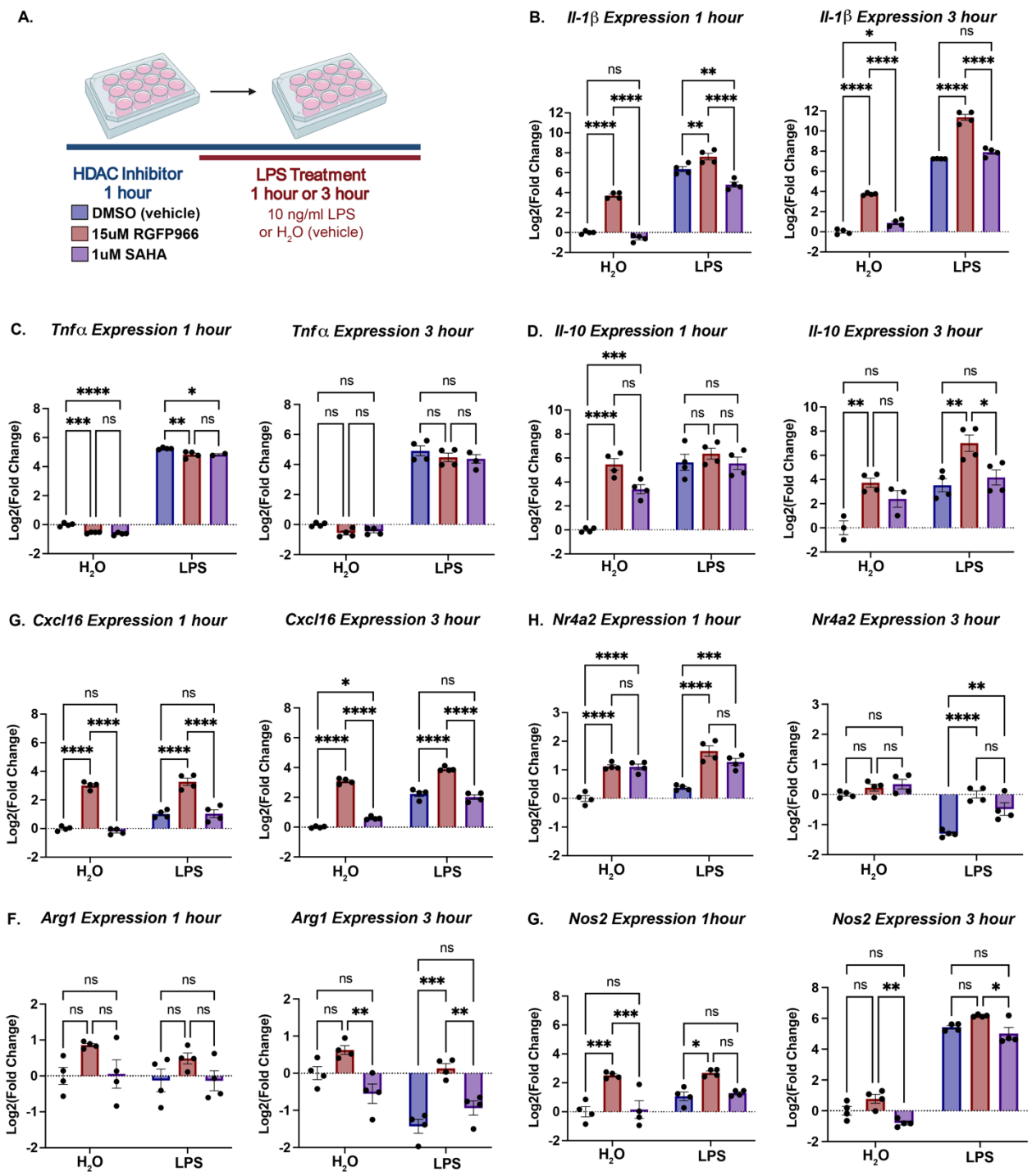

Figure 2. Hdac inhibition modulates LPS regulated gene expression

(A) Experimental design for testing the role of Hdacs in modulating LPS regulated gene expression in BV2 cultures. For all subsequent panels DMSO control is shown in blue, RGFP966 shown in red and SAHA in purple. (B) *Il-1b* expression is enhanced by Hdac3 inhibition at baseline and in response to LPS at 1 and 3 hours of treatment. (C) Tnfa expression is slightly repressed by Hdac inhibition at 1 hour and unmodulated at 3 hours of LPS treatment. (D) *Il-10* expression is enhanced by Hdac3 inhibition at baseline and in response to LPS at 3 hours of

treatment. (E) *Cxcl16* expression is enhanced by Hdac3 inhibition at baseline and in response to LPS at 1 and 3 hours of treatment. (F) *Nr4a2* expression is enhanced by both RGFP966 and SAHA at baseline and in response to LPS at 1 hour. Both RGFP966 and SAHA prevent the normal, LPS induced repression of *Nr4a2* expression at 3 hours of LPS. (G) *Arg1* expression is not above baseline in any condition at 1 hour of LPS treatment. At 3 hours, RGFP966, but not SAHA, blocks LPS induced repression of *Nr4a2*. (H) At 1 hour LPS, *Nos2* expression is increased by Hdac3 inhibition, but not SAHA, under baseline conditions and in response to LPS. At 3 hours expression largely matches DMSO treated controls. Each panel is Log2 fold change relative to DMSO control treated with water and error bars are +/- SEM. In all panels DMSO water versus DMSO LPS significance is not shown, but reaches statistical threshold (*p<0.05) for all genes at 1 hour of LPS except *Nr4a2*, *Arg1*, and *Nos2* and was significant for all genes at 3 hours LPS. n=3-4 per condition in at least 3 independent replication experiments. *p<0.05, **p<.01, ***p<0.001, ****p<0.0001.

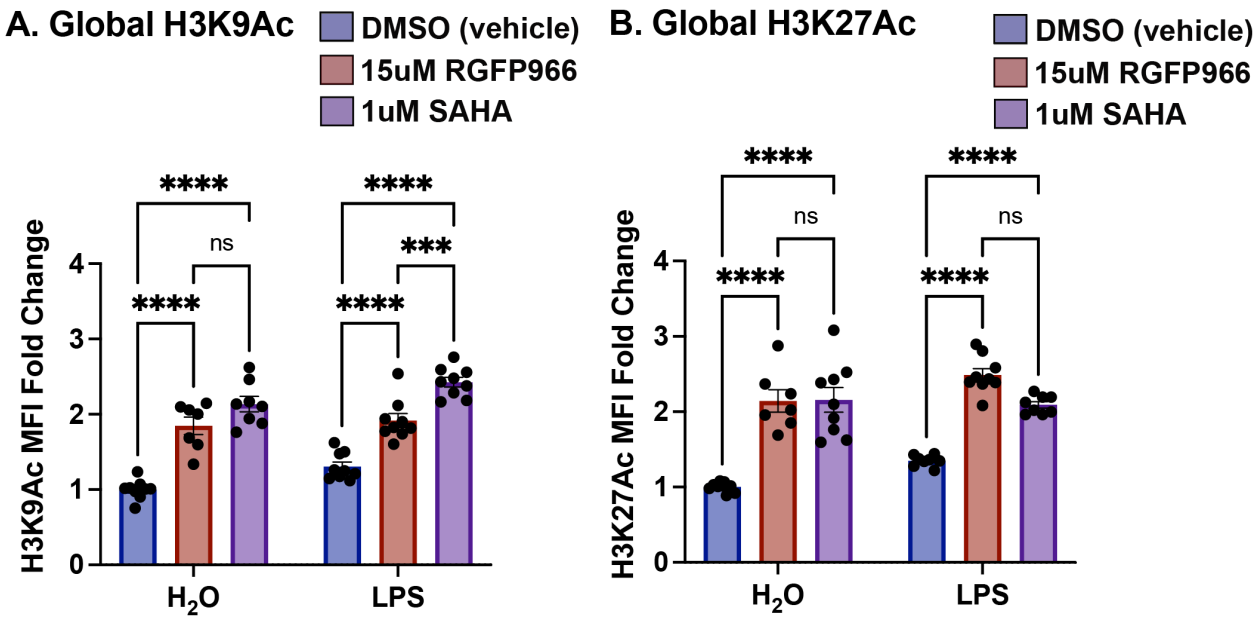

Figure 3. Global changes in histone acetylation upon Hdac inhibition

BV2 microglial cells were treated with DMSO, RGFP966 or SAHA for 1 hour and then either water or LPS was added for three hours. Cells were then harvested and intracellular staining was performed for H3K9ac or H3K27ac. (A) Global levels of H3K9ac were significantly increased with both RGFP966 and SAHA at baseline and upon LPS treatment. (B) H3K27ac levels were increased with both RGFP966 and SAHA at baseline and upon LPS treatment. The magnitude of increase was similar with the two Hdac inhibitors. Tukey's corrected posthocs *p<0.05, **p<0.005, ***p<0.001, ****p<0.0001. MFI: median fluorescence intensity. Fold change is relative to DMSO treated water samples. n=5-6 per treatment in 3 independent replication experiments.

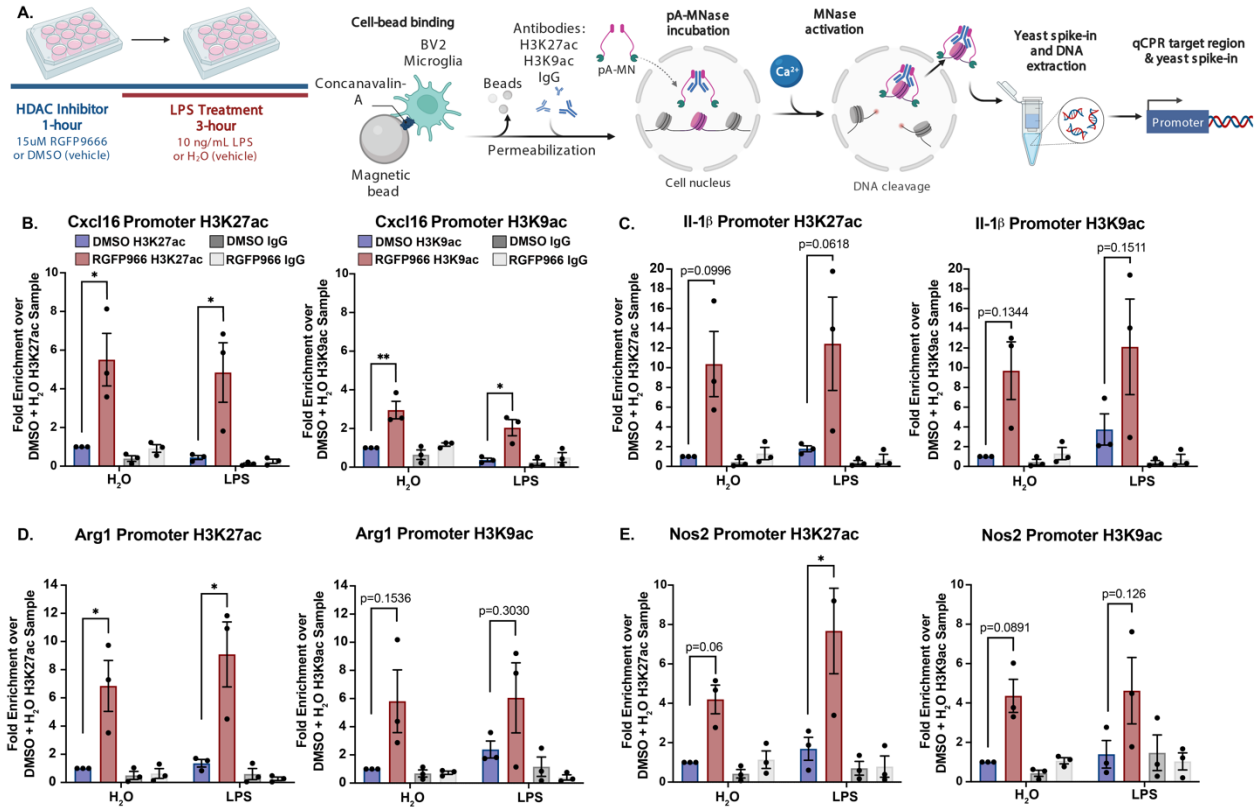

Figure 4. Histone acetylation changes at Hdac3 modulated genes

(A) Experimental design for CUT&RUN qPCR analysis of H3K27ac and H3K9ac over promoters of key Hdac regulated target genes. All samples are normalized to yeast spike in and expressed as a percentage of input sample based on standard curve. Signal then calculated as fold enrichment relative to the H3K27ac or H3K9ac antibody levels in the DMSO and water treated control. DMSO and RGFP966 non-immune IgG samples were included for all experiments (B) H3K27ac and H3K9ac signal is significantly increased over the Cxcl16 promoter with RGFP966 treatment. (B) Trends for increased H3K27ac and H3K9ac signal with RGFP966 over the Il1-b promoter. (C) H3K27ac signal is significantly increased over the Arg1 promoter with RGFP966 treatment. H3K9ac shows similar trends but did not reach significance. (D) H3K27ac signal is significantly increased over the Nos2 promoter with RGFP966 and LPS treatment. H3K9ac shows similar trends but did not reach significance. All plots are fold enrichment with +/- SEM. n=3 per condition in independent replication experiments. *p<0.05.

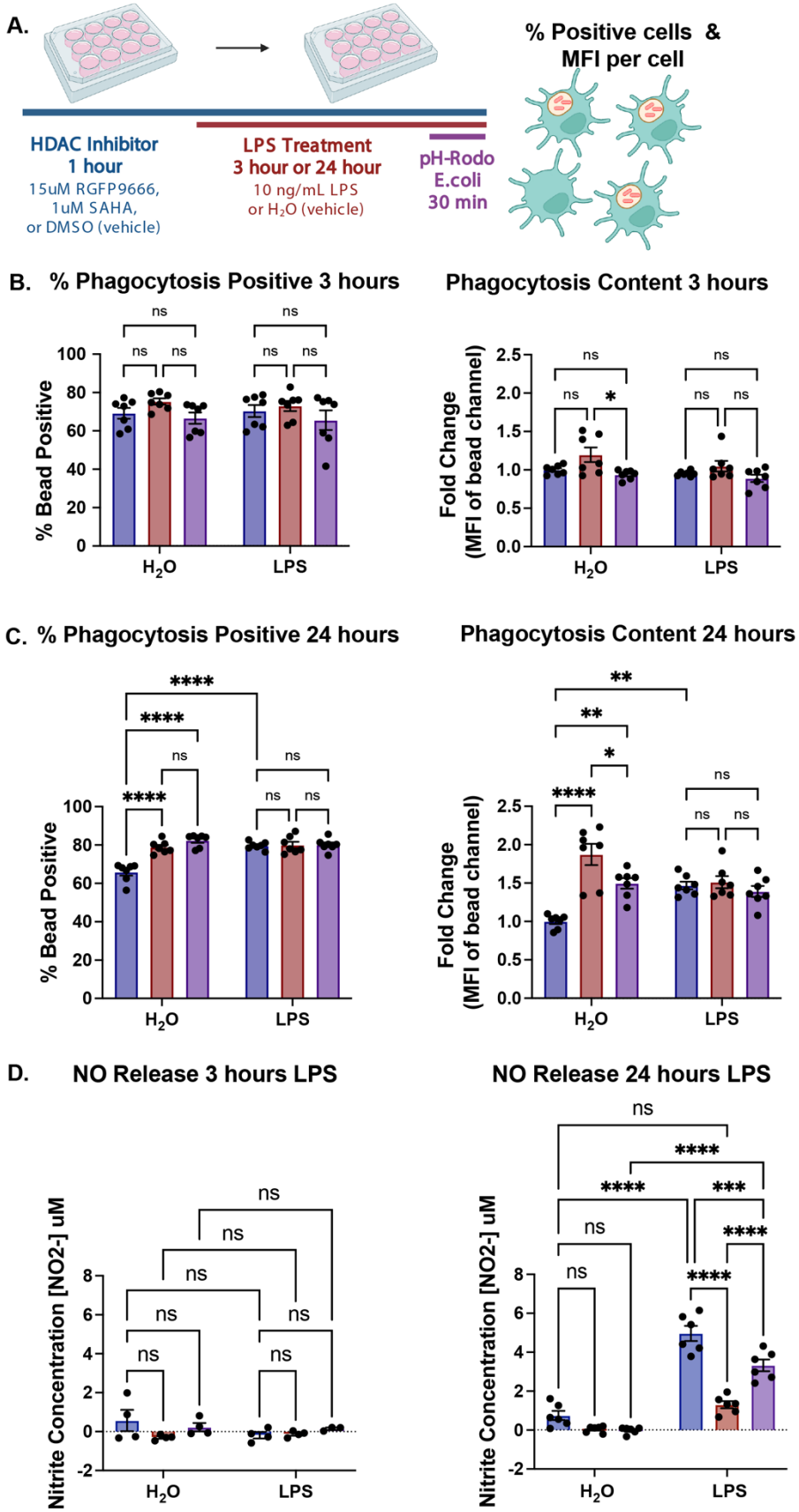
A.
% Positive cells & MFI per cell
HDAC Inhibitor
1 hour
15uM RGFP9666,
1uM SAHA,
or DMSO (vehicle)
LPS Treatment
3 hour or 24 hour
10 ng/mL LPS
or H2O (vehicle)
pH-Rodo
E.coli
30 min
B. % Phagocytosis Positive 3 hours
% Bead Positive
H2O
LPS
Phagocytosis Content 3 hours
Fold Change
(MFI of bead channel)
C. % Phagocytosis Positive 24 hours
Phagocytosis Content 24 hours
D. NO Release 3 hours LPS
NO Release 24 hours LPS
Nitrite Concentration [NO2-] uM

Figure 5. Hdac inhibition enhances microglial phagocytosis and suppresses nitric oxide release
(A) Experimental design for phagocytosis assay. Both the percent of positive microglia and the MFI per microglia are quantified by flow cytometry (B) Hdac inhibition shows minimal impacts on phagocytosis of pH-rodo *E. coli* tagged beads at 3 hours of LPS treatment. (C) Hdac inhibition enhances phagocytosis at baseline after 24 hours, bringing the percent of positive microglia to LPS levels. (D) Hdac inhibition enhances phagocytosis at baseline after 24 hours, bringing it above LPS induced levels in the case of RGFP966. (E) Minimal release of NO after 3 hours of LPS. (E) At 24 hours of LPS treatment, DMSO treated samples show a significant increase in NO release. This effect was blunted with SAHA and completely repressed to baseline levels with RGFP966. Mean +/- SEM. n=4-7 from 2 or 3 independent experiments. *p<0.05, **p<.01, ***p<0.001, ****p<0.0001.

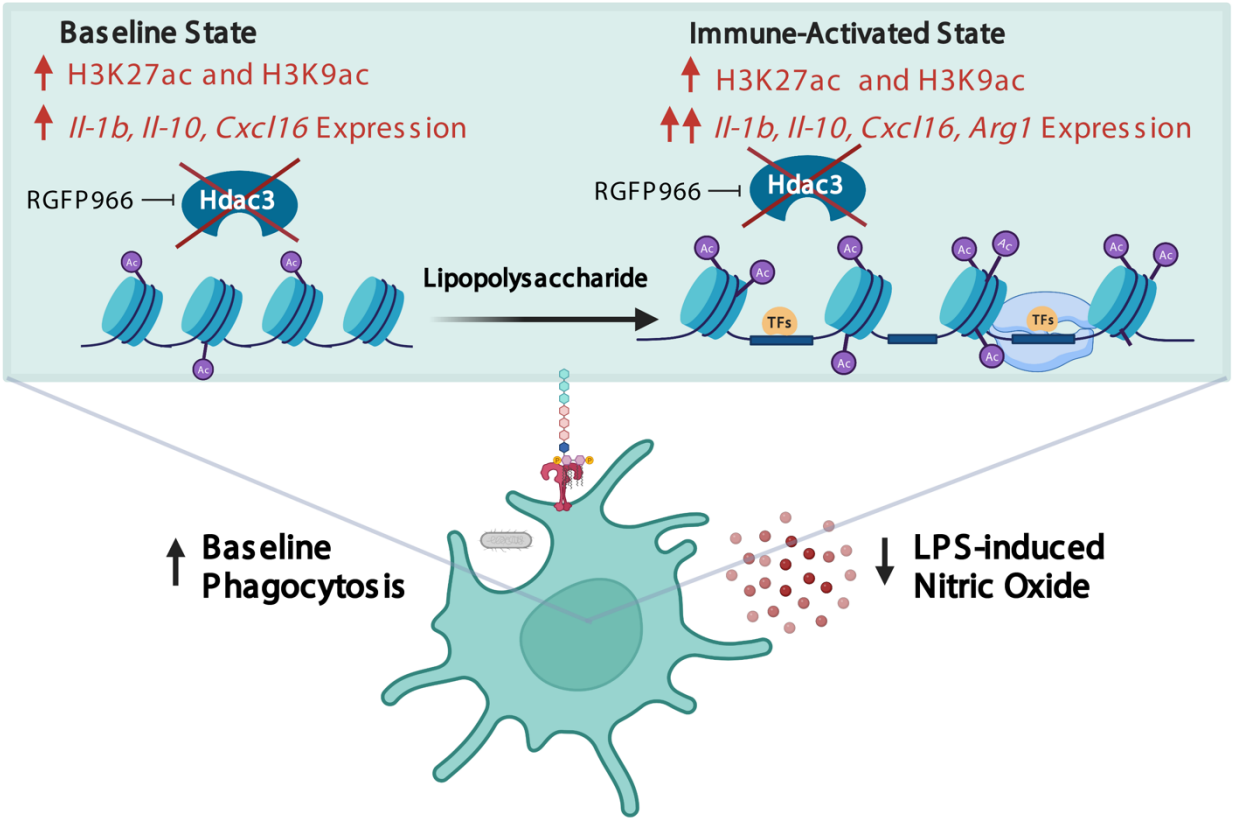

Figure 6. Model for Hdac3 regulation of microglial LPS mediated gene expression and function
Hdac3 represses baseline gene expression through deacetylation of H3K27ac and H3K9ac marked histones. Upon LPS stimulation Hdac3 releases, allowing for increased histone acetylation and immune activation. In the presence of RGFP966, Hdac3's deacetylase activity is blocked allowing for increased histone acetylation at baseline and an aberrant increase in baseline gene expression. Upon LPS, inhibition of Hdac3 results in hyper-induction of Hdac3 target genes and a lack of suppression of genes normally repressed by LPS treatment. These

gene expression shifts ultimately culminate in increased phagocytosis and repressed NO release, driving microglia towards a phenotype that promotes resolution of inflammation.

Conflict of Interest

The authors declare that the research was conducted in the absence of any commercial or financial relationships that could be construed as a potential conflict of interest.

Author Contributions

LM and AC conceived of the project and experimental design, analyzed data and wrote the manuscript. MT conducted and analyzed flow cytometry experiments. VB, JK and MR assisted with experiments and analysis. All authors contributed to the manuscript.

Funding

This work was supported by the Canadian Institutes for Health Research [CRC-RS 950-232402 to AC and Canada Graduate Scholarship-Master's to LM]; Natural Sciences and Engineering Research Council of Canada [RGPIN-2019-04450, DGECR-2019-00069 to AC]; and Scottish Rite Charitable Foundation [21103 to AC]. The funders had no role in study design, data collection and analysis, decision to publish, or preparation of the manuscript.

References

Anja Henn, Søren Lund, Maj Hedtjärn, André Schrattenholz, Peter Pörzgen ML (2009) The Suitability of BV2 Cells as Alternative Model System for Primary Microglia Cultures or for Animal Experiments Examining Brain Inflammation. Altex 26:83–94.

Bennett FC, Bennett ML, Yaqoob F, Mulinyawe SB, Grant GA, Hayden Gephart M, Plowey ED, Barres BA (2018) A Combination of Ontogeny and CNS Environment Establishes Microglial Identity. Neuron 98:1170-1183.e8.

Bian HT, Xiao L, Liang L, Xie YP, Wang HL, Wang GH (2021) RGFP966 is protective against lipopolysaccharide-induced depressive-like behaviors in mice by inhibiting neuroinflammation and microglial activation. International Immunopharmacology 101.

Campbell RR, Kramár EA, Pham L, Beardwood JH, Augustynski AS, López AJ, Chitnis OS, Delima G, Banihani J, Matheos DP, Wood MA (2021) HDAC3 Activity within the Nucleus Accumbens Regulates Cocaine-Induced Plasticity and Behavior in a Cell-Type-Specific Manner. The Journal of neuroscience : the official journal of the Society for Neuroscience 41:2814–2827.

Chen LF, Fischle W, Verdin E, Greene WC (2001) Duration of nuclear NF-κB action regulated by reversible acetylation. Science 293:1653–1657.

Chen X, Barozzi I, Termanini A, Prosperini E, Recchiuti A, Dalli J, Mietton F, Matteoli G, Hiebert S, Natoli G (2012) Requirement for the histone deacetylase Hdac3 for the inflammatory

gene expression program in macrophages. Proceedings of the National Academy of Sciences 109:E2865–E2874.

Cherry JD, Olschowka JA, O'Banion MK (2014) Neuroinflammation and M2 microglia: The good, the bad, and the inflamed. Journal of Neuroinflammation 11:1–15.

Chuang HC, Chang CW, Chang GD, Yao TP, Chen H (2006) Histone deacetylase 3 binds to and regulates the GCMa transcription factor. Nucleic Acids Research 34:1459.

Cronk JC, Filiano AJ, Louveau A, Marin I, Marsh R, Ji E, Goldman DH, Smirnov I, Geraci N, Acton S, Overall CC, Kipnis J (2018) Peripherally derived macrophages can engraft the brain independent of irradiation and maintain an identity distinct from microglia. The Journal of experimental medicine:jem.20180247.

Datta M, Staszewski O, Raschi E, Frosch M, Hagemeyer N, Tay TL, Blank T, Kreutzfeldt M, Merkler D, Ziegler-Waldkirch S, Matthias P, Meyer-Luehmann M, Prinz M (2018) Histone Deacetylases 1 and 2 Regulate Microglia Function during Development, Homeostasis, and Neurodegeneration in a Context-Dependent Manner. Immunity 48:514-529.e6.

De Jager PL et al. (2009) Meta-analysis of genome scans and replication identify CD6, IRF8 and TNFRSF1A as new multiple sclerosis susceptibility loci. Nature Genetics 41:776–782.

Ghiboub M, Zhao J, Li Yim AYF, Schilderink R, Verseijden C, van Hamersveld PHP, Duarte JM, Hakvoort TBM, Admiraal I, Harker NR, Tough DF, Henneman P, de Winther MPJ, de Jonge WJ (2020) HDAC3 Mediates the Inflammatory Response and LPS Tolerance in Human Monocytes and Macrophages. Frontiers in Immunology 11:2608.

Gosselin D, Link VM, Romanoski CE, Fonseca GJ, Eichenfield DZ, Spann NJ, Stender JD, Chun HB, Garner H, Geissmann F, Glass CK (2014) Environment drives selection and function of enhancers controlling tissue-specific macrophage identities. Cell 159:1327–1340.

Gosselin D, Skola D, Coufal NG, Holtman IR, Schlachetzki JCM, Sajti E, Jaeger BN, O'Connor C, Fitzpatrick C, Pasillas MP, Pena M, Adair A, Gonda DG, Levy ML, Ransohoff RM, Gage FH, Glass CK (2017) An environment-dependent transcriptional network specifies human microglia identity. Science Jun 23:6344.

Grégoire S, Xiao L, Nie J, Zhang X, Xu M, Li J, Wong J, Seto E, Yang X-J (2007) Histone deacetylase 3 interacts with and deacetylates myocyte enhancer factor 2. Molecular and cellular biology 27:1280–1295.

Guenther MG, Barak O, Lazar MA (2001) The SMRT and N-CoR Corepressors Are Activating Cofactors for Histone Deacetylase 3 The SMRT and N-CoR Corepressors Are Activating Cofactors for Histone Deacetylase 3. 21.

Guerreiro R et al. (2013) TREM2 Variants in Alzheimer's Disease . New England Journal of Medicine 368:117–127.

Hammond TR, Dufort C, Dissing-Olesen L, Giera S, Young A, Wysoker A, Walker AJ, Gergits F, Segel M, Nemesh J, Marsh SE, Saunders A, Macosko E, Ginhoux F, Chen J, Franklin RJM, Piao X, McCarroll SA, Stevens B (2018a) Single-Cell RNA Sequencing of Microglia throughout the Mouse Lifespan and in the Injured Brain Reveals Complex Cell-State Changes. Immunity 0.

Hammond TR, Robinton D, Stevens B (2018b) Microglia and the Brain: Complementary Partners in Development and Disease. Annual review of cell and developmental biology 34:523–544.

Hollingworth P et al. (2011) Common variants at ABCA7, MS4A6A/MS4A4E, EPHA1, CD33 and CD2AP are associated with Alzheimer's disease. Nature Genetics 43:429–436.

Hsing CH, Hung SK, Chen YC, Wei TS, Sun DP, Wang JJ, Yeh CH (2015) Histone deacetylase inhibitor trichostatin a ameliorated endotoxin-induced neuroinflammation and cognitive dysfunction. Mediators of Inflammation 2015.

Ishii S (2021) The Role of Histone Deacetylase 3 Complex in Nuclear Hormone Receptor Action. International journal of molecular sciences 22.

Kacimi R, Giffard RG, Yenari MA (2011) Endotoxin-activated microglia injure brain derived endothelial cells via NF-κB, JAK-STAT and JNK stress kinase pathways. Journal of Inflammation 8:7.

Kaikkonen MU, Spann NJ, Heinz S, Romanoski CE, Allison K a., Stender JD, Chun HB, Tough DF, Prinjha RK, Benner C, Glass CK (2013) Remodeling of the enhancer landscape during macrophage activation is coupled to enhancer transcription. Molecular Cell 51:310–325.

Karagianni P, Wong J (2007) HDAC3: taking the SMRT-N-CoRrect road to repression. Oncogene 26:5439–5449.

Kierdorf K et al. (2013) Microglia emerge from erythromyeloid precursors via Pu.1- and Irf8-dependent pathways. Nature neuroscience 16:273–280.

Kuboyama T, Wahane S, Huang Y, Zhou X, Wong JK, Koemeter-Cox A, Martini M, Friedel RH, Zou H (2017) HDAC3 inhibition ameliorates spinal cord injury by immunomodulation. Scientific Reports 7:1–13.

Kwapis JL, Alaghband Y, Kramár EA, López AJ, Vogel Ciernia A, White AO, Shu G, Rhee D, Michael CM, Montellier E, Liu Y, Magnan CN, Chen S, Sassone-Corsi P, Baldi P, Matheos DP, Wood MA (2018) Epigenetic regulation of the circadian gene Per1 contributes to age-related changes in hippocampal memory. Nature Communications 9:3323.

Lavin Y, Winter D, Blecher-Gonen R, David E, Keren-Shaul H, Merad M, Jung S, Amit I (2014) Tissue-resident macrophage enhancer landscapes are shaped by the local microenvironment. Cell 159:1312–1326.

Leppä V et al. (2011) The genetic association of variants in CD6, TNFRSF1A and IRF8 to multiple sclerosis: A multicenter case-control study. PLoS ONE 6.

Li J, Wang J, Wang J, Nawaz Z, Liu JM, Qin J, Wong J (2000) Both corepressor proteins SMRT and N-CoR exist in large protein complexes containing HDAC3. EMBO Journal 19:4342–4350.

Li Q, Cheng Z, Zhou L, Darmanis S, Neff NF, Okamoto J, Gulati G, Bennett ML, Sun LO, Clarke LE, Marschallinger J, Yu G, Quake SR, Wyss-Coray T, Barres BA (2019) Developmental Heterogeneity of Microglia and Brain Myeloid Cells Revealed by Deep Single-Cell RNA Sequencing. Neuron.

Malvaez M, Greenfield VY, Matheos DP, Angelillis NA, Murphy MD, Kennedy PJ, Wood MA, Wassum KM (2018) Habits Are Negatively Regulated by Histone Deacetylase 3 in the Dorsal Striatum. Biological psychiatry 84:383–392.

Malvaez M, McQuown SC, Rogge GA, Astarabadi M, Jacques V, Carreiro S, Rusche JR, Wood MA (2013) HDAC3-selective inhibitor enhances extinction of cocaine-seeking behavior in a persistent manner. Proceedings of the National Academy of Sciences of the United States of America 110:2647–2652.

Marks PA (2007) Discovery and development of SAHA as an anticancer agent. Oncogene 26:1351–1356.

Mcquown SC, Wood MA (2011) Neurobiology of Learning and Memory HDAC3 and the molecular brake pad hypothesis. Neurobiology of Learning and Memory 96:27–34.

McQuown SC, Wood MA (2011) HDAC3 and the molecular brake pad hypothesis. Neurobiology of Learning and Memory 96:27–34.

Mullican SE, Gaddis CA, Alenghat T, Nair MG, Giacomin PR, Everett LJ, Feng D, Steger DJ, Schug J, Artis D, Lazar MA (2011) Histone deacetylase 3 is an epigenomic brake in macrophage alternative activation. Genes and Development 25:2480–2488.

Nguyen HCB, Adlanmerini M, Hauck AK, Lazar MA (2020) Dichotomous engagement of HDAC3 activity governs inflammatory responses. Nature 584:286–290.

Park TJ, Kim HJ, Kim JH, Bae JS, Cheong HS, Park BL, Shin HD (2013) Associations of CD6, TNFRSF1A and IRF8 polymorphisms with risk of inflammatory demyelinating diseases. Neuropathology and Applied Neurobiology 39:519–530.

Phan ML, Gergues MM, Mahidadia S, Jimenez-Castillo J, Vicario DS, Bieszczad KM (2017) HDAC3 Inhibitor RGFP966 Modulates Neuronal Memory for Vocal Communication Signals in a Songbird Model. Frontiers in systems neuroscience 11.

Pollock TB, Cholico GN, Isho NF, Day RJ, Suresh T, Stewart ES, McCarthy MM, Rohn TT (2020) Transcriptome Analyses in BV2 Microglial Cells Following Treatment With Amino-Terminal Fragments of Apolipoprotein E. Frontiers in Aging Neuroscience 12:1–15.

Prinz M, Masuda T, Wheeler MA, Quintana FJ (2021) Microglia and Central Nervous System–Associated Macrophages—From Origin to Disease Modulation. https://doi.org/101146/annurev-immunol-093019-110159 39:251–277.

Sekar A, Bialas AR, De Rivera H, Davis A, Hammond TR, Kamitaki N, Tooley K, Presumey J, Baum M, Van Doren V, Genovese G, Rose SA, Handsaker RE, Daly MJ, Carroll MC, Stevens B, McCarroll SA (2016) Schizophrenia risk from complex variation of complement component 4. Nature 530:177–183.

Shemer A, Grozovski J, Tay TL, Tao J, Volaski A, Süß P, Ardura-Fabregat A, Gross-Vered M, Kim JS, David E, Chappell-Maor L, Thielecke L, Glass CK, Cornils K, Prinz M, Jung S (2018) Engrafted parenchymal brain macrophages differ from microglia in transcriptome, chromatin landscape and response to challenge. Nature Communications 2018 9:1 9:1–16.

Sims R, Badarinarayan N, Raybould R, Heilmann-Heimbach S, Vronskaya M, Hoffmann P (2017) Rare coding variants in PLCG2, ABI3 and TREM2 implicate microglial-mediated innate immunity in Alzheimer's disease. Nature Genetics 49:1373–1384.

Talbert PB, Henikoff S (2021) The Yin and Yang of Histone Marks in Transcription. Annual Review of Genomics and Human Genetics 22:147–170.

Vogel-Ciernia A, Wood M (2012) Molecular brake pad hypothesis: pulling off the brakes for emotional memory. Reviews in the Neurosciences 23:607–626.

Wahane S, Zhou X, Zhou X, Guo L, Friedl MS, Kluge M, Ramakrishnan A, Shen L, Friedel CC, Zhang B, Friedel RH, Zou H (2021) Diversified transcriptional responses of myeloid and glial cells in spinal cord injury shaped by HDAC3 activity. Science Advances 7:8811–8837.

Wendeln A-C et al. (2018) Innate immune memory in the brain shapes neurological disease hallmarks. Nature 556:332–338.

Yang L, Chen S, Zhao Q, Pan C, Peng L, Han Y, Li L, Ruan J, Xia J, Yang H, Xu F, Cheng G (2022) Histone deacetylase 3 contributes to the antiviral innate immunity of macrophages by interacting with FOXK1 to regulate STAT1/2 transcription. Cell Reports 38:110302.

Yang Z, Ming XF (2014) Functions of arginase isoforms in macrophage inflammatory responses: Impact on cardiovascular diseases and metabolic disorders. Frontiers in Immunology 5:1–10.

Zhang MJ, Zhao QC, Xia MX, Chen J, Chen YT, Cao X, Liu Y, Yuan ZQ, Wang XY, Xu Y (2020) The HDAC3 inhibitor RGFP966 ameliorated ischemic brain damage by downregulating the AIM2 inflammasome. FASEB Journal 34:648–662.

Zhao Y, Mu H, Huang Y, Li S, Wang Y, Stetler RA, Bennett MVL, Dixon CE, Chen J, Shi Y (2022) Microglia-specific deletion of histone deacetylase 3 promotes inflammation resolution, white matter integrity, and functional recovery in a mouse model of traumatic brain injury. Journal of Neuroinflammation 19:201.